Sustainable Energy & Fuels

Modification of gold nanoparticles with a hole-transferring cocatalyst: A new strategy for plasmonic water splitting under irradiation of visible light

Journal:	*Sustainable Energy & Fuels*
Manuscript ID	SE-ART-03-2021-000367.R1
Article Type:	Paper
Date Submitted by the Author:	29-Apr-2021
Complete List of Authors:	Fudo, Eri; Kindai University, Applied Chemistry Tanaka, Atsuhiro; Kindai Univ., Applied Chemistry Iguchi, Shoji; Tokyo Institute of Technology School of Materials and Chemical Technology , Department of Chemical Science and Engineering Kominami, Hiroshi; Kindai University, Applied Chemistry

ARTICLE

Modification of gold nanoparticles with a hole-transferring cocatalyst: A new strategy for plasmonic water splitting under irradiation of visible light

Received 00th January 20xx,
Accepted 00th January 20xx

DOI: 10.1039/x0xx00000x

Eri Fudo[1], Atsuhiro Tanaka[2, 3], Shoji Iguchi[4], Hiroshi Kominami[2*]

Plasmonic water splitting ($H_2O \rightarrow H_2 + 1/2O_2$) over a metal-loaded metal oxide under irradiation of visible light is still difficult, although conversion of organic compounds over plasmonic photocatalysts has become popular. Acceleration of oxygen (O_2) production by water oxidation is a key for smooth water splitting. A chromium species was introduced to gold (Au)-loaded titanium(IV) oxide (Au/TiO_2) by using a photodeposition method. The morphology, structure and electronic state of the chromium species and Au/TiO_2 were analyzed by transmission electron microscopy, UV-vis spectroscopy, X-ray photoelectron spectroscopy and X-ray absorption spectroscopy. The results revealed that a very thin chromium hydroxide ($Cr(OH)_3$) layer formed on Au nanoparticles, which made the state of Au slightly electron-rich. The $Cr(OH)_3/Au/TiO_2$ plasmonic photocatalyst exhibited reaction rates larger than those over $Cr(OH)_3$-free Au/TiO_2 in both water oxidation and water splitting under irradiation of visible light. Oxidative deposition of PbO_2 revealed that plasmonic oxidation occurs on $Cr(OH)_3/Au$ and that $Cr(OH)_3$ effectively works as the hole transfer cocatalyst. Based on the results, reaction mechanisms of plasmonic water oxidation and water splitting over $Cr(OH)_3/Au/TiO_2$ are proposed.

Introduction

Photocatalytic water splitting has attracted much interest as an ideal way for hydrogen (H_2) production under abundant solar light.[1] In the past few decades, many photocatalysts that have the ability to evolve H_2 and oxygen (O_2) from water have been reported. Domen and Kudo's group reported that water splitting ($H_2O \rightarrow H_2 + 1/2O_2$) occurs over some oxide photocatalysts having a perovskite structure such as $SrTiO_3$ and $NaTaO_3$.[2, 3] Since $SrTiO_3$ has a sufficient potential for reduction of protons (H^+), no external potential is needed to produce H_2. In addition, $SrTiO_3$ and $NaTaO_3$ modified with nickel oxide (NiO_x) decompose pure water because NiO_x does not work for a back reaction of water splitting. Besides the above examples, many researchers have developed water splitting systems including oxide photocatalysts[4], metal-organic framework[5] and Z-scheme.[6, 7] Water splitting consists of two half-reactions: 1) reduction of H^+ ($2H^+ + 2e^- \rightarrow H_2$) and 2) water ($H_2O$) oxidation ($2H_2O \rightarrow O_2 + 4H^+ + 4e^-$). In a water splitting system, it is known that H_2O oxidation is the rate-determining step because this reaction requires four electrons to produce O_2.[8, 9] Hence, it is important to improve the photocatalytic activity of water oxidation for artificial photosynthesis. Maeda *et al*. reported that titanium-based semiconductors (TiO_2) modified with cobalt oxide nanoparticles (NPs) work as water oxidation photocatalysts under irradiation of visible light (up to 850 nm) in the presence of silver ions (Ag^+). [10]

A plasmonic photocatalyst is a new type of photocatalyst responding to visible light. Gold (Au) NPs loaded on titanium(IV) oxide (TiO_2), cerium(IV) oxide and tungsten(VI) oxide showed photoabsorption at around 550 nm due to localized surface plasmon resonance (LSPR) and have been applied to various chemical reactions such as decomposition of organic substrates [11, 12, 13, 14, 15], selective oxidation of aromatic alcohol to a carbonyl compound[16, 17, 18], H_2 formation from alcohols[19, 20, 21, 22], selective reduction of organic compounds[18, 23] and water splitting[24]. Our research group achieved water oxidation over TiO_2 modified with Au and platinum NPs in the presence of an electron donor under irradiation of visible light[25]. We also achieved water splitting over Au/TiO_2 modified with NiO_x as a cocatalyst for reduction of H^+ under irradiation of visible light ($\lambda < 700$ nm)[24]. Other researchers have reported plasmonic water oxidation to enhance photocatalytic activities of water splitting. Li *et al.* performed water oxidation over Au/TiO_2 and *ca*. 30 μmol of O_2 was produced for 6 h of photoirradiation. They also investigated oxidation of lead(II) in an aqueous suspension of an Au/TiO_2 plasmonic photocatalyst and observed deposition of lead(IV) oxide at the interface of Au and TiO_2 by using a Kelvin probe force microscope. Their results indicate that the oxidation process occurs at the interface of Au and TiO_2, *i.e.*,

[1]*Department of Molecular and Material Engineering, Graduate School of Science and Engineering, Kindai University, Kowakae, Higashiosaka, Osaka 577-8502, Japan*
[2]*Department of Applied Chemistry, Faculty of Science and Engineering, Kindai University, Kowakae, Higashiosaka, Osaka 577-8502, Japan*
[3]*Precursory Research for Embryonic Science and Technology (PRESTO), Japan Science and Technology Agency (JST), Honcho, Kawaguchi 332-0012, Japan.*
[4]*Department of Chemical Science and Engineering, School of Materials and Chemical Technology, Tokyo Institute of Technology, Ookayama, Meguro-ku, Tokyo 152-8550 Japan*
*Email: hiro@apch.kindai.ac.jp
Electronic Supplementary Information (ESI) available: Discussion about effect of amount of $Cr(OH)_3$, Figures S1-S10. See DOI: 10.1039/x0xx00000x

plasmon-induced hot holes are located at the interface of Au and TiO_2.[26] Minamimoto *et al.* first visualized oxidation site of Au/TiO_2 plasmonic system by means of photoelectrochemical methods.[27] Misawa *et al.* reported that O_2 and hydrogen peroxide were evolved from Au nanorods (NRs) fabricated on TiO_2 (Au NRs/TiO_2) with near-infrared light (λ: 1000 nm) and *ca*. 83 μmol of O_2 was evolved at 0.3 V a saturated calomel electrode. The action spectrum of the photocurrent corresponded to an extinction spectrum of Au NRs/TiO_2, indicating that a plasmonic photocurrent was generated by irradiating visible to near-infrared light.[28] Since water oxidation often controls the reaction rate of water splitting as mentioned above, acceleration of this process over plasmonic photocatalysts is also very important.

Cobalt oxide (CoO_x)[29] and chromium oxide (Cr_2O_3)[30] have been used as effective materials for hole transfer in photoelectrochemistry in addition to g-C_3N_4.[31] Nurlaela *et al*.[29] reported that photocatalytic oxygen evolution reaction (OER) over a CoO_x-modified tantalum nitride (Ta_3N_5) particulate was improved by adding trace amounts (~0.05 wt %) of noble metals (Rh and Ru) to CoO_x. Sekizawa *et al*.[18][30] reported that insertion of a thin Cr_2O_3 layer between transparent conductive oxide and N, Zn-codoped Fe_2O_3 layers enhanced the cathodic photocurrent. Tatsuma *et al*.[32] investigated the combinations of a TiO_2-Au photoelectrode and p-type semiconductors such as nickel hydroxide $Ni(OH)_2$ and CrO_x. They found that TiO_2-Au-$Ni(OH)_2$ and TiO_2-Au-CrO_x photoelectrodes show efficient plasmon-induced charge separation under visible light and accumulate positive charges released from resonant Au nanoparticles. They reported that the TiO_2-Au-$Ni(OH)_2$ electrode shows much stronger photoresponses than those of the TiO_2-Au-CrO_x electrode and that the former produces *ca*. 0.2 μmol of oxygen by water oxidation under irradiation of visible light for 2.5 h with a certain bias voltage (0.2 V vs. Ag/AgCl). Very recently, Okazaki *et al.* reported that site-selectively deposited CoO_x on Au/TiO_2 electrode improved photoelectrochemical water oxidation activity due to the function of CoO_x cocatalyst. The CoO_x/Au/TiO_2 thin film anode produced *ca.* 8 μmol of O_2 for 5 h at -0.31 V vs. Ag/AgCl under simulated sunlight (100 mW cm^{-2}).[33]

In this study, we investigated whether a hole transfer cocatalyst is effective for the H_2O oxidation process over an Au plasmonic photocatalyst in a powder suspension system. We chose chromium(III) species (identified as $Cr(OH)_3$ in this study) as the hole transfer cocatalyst because chromium(III) species can be easily introduced to an Au/TiO_2 plasmonic photocatalyst through reductive photodeposition (PD) using chromium(VI) species. The $Cr(OH)_3/Au/TiO_2$ samples prepared were characterized by using various techniques and then used for plasmonic water oxidation (O_2 evolution) and water splitting (to H_2 and O_2) under irradiation of visible light in the presence and absence of an electron acceptor. Here we report the results of characterization and activity tests of Au/TiO_2 and $Cr(OH)_3/Au/TiO_2$ samples and then discuss the function of $Cr(OH)_3$ and the mechanisms of plasmonic water oxidation and water splitting.

Experimental

2.1. Preparation of Au/TiO_2 and $Cr(OH)_3/Au/TiO_2$

All of the reagents were commercial materials of reagent grade and were used without further purification. Commercial TiO_2 powder (P25) with an anatase/rutile phase was supplied by Degussa. Loading of Au on TiO_2 was performed by the photodeposition (PD) method. TiO_2 powder (114 mg) was suspended in 10 cm^3 of an aqueous solution of methanol (10 vol%) in a test tube, and then an aqueous solution of tetrachloroauric acid (as 1.2 mg Au) was added. The test tube was sealed with a rubber septum under argon (Ar) and then photoirradiated for 1 h at λ> 300 nm by a 400 W high-pressure mercury arc (Koike Precision Instruments, Hyogo) under Ar with magnetic stirring in a water bath continuously kept at 298 K. The Au source was reduced by photogenerated electrons, and Au metal was deposited on TiO_2 particles, resulting in the formation of Au/TiO_2. After photodeposition of Au, a solution of potassium dichromate (y = 0.05, 0.10, 0.20, 0.25, 0.50, and 1.00 wt %) was injected into the reaction mixture, and the mixture was photoirradiated by the same mercury arc under the same conditions as those for preparation of the Au(1.0)/TiO_2 sample. Under this condition, $Cr(OH)_3$ was deposited reductively. Analysis of the liquid phase after photodeposition revealed that the Au and Cr sources had been almost completely (>99.9%) deposited as Au and $Cr(OH)_3$ on the TiO_2 particles. The resultant powder was washed repeatedly with distilled water and then dried at 298 K in vacuo for 2 h. Thus-prepared sample is shown as $Cr(OH)_3$(y)/Au(1.0)/TiO_2.

2.2 Characterization

Morphology of the Au/TiO_2 and $Cr(OH)_3/Au/TiO_2$ samples was observed under a JEOL JEM-2100F transmission electron microscope (TEM) operated at 200 kV in the Joint Research Center at Kindai University (JRC). X-ray photoelectron spectroscopy (XPS) spectra of Au/TiO_2, $Cr(OH)_3/Au/TiO_2$, and $Cr(OH)_3/TiO_2$ were measured using AXIS-NOVA ESCA (Shimadzu, Kyoto) in JRC. A sample was mounted on a silver sample holder by using conductive carbon tape and was analyzed using Al Kα radiation in a vacuum chamber in 0.1-eV steps. The position of the carbon peak (284.6 eV) for C 1s was used to calibrate the binding energy for all of the samples. Diffuse reflectance spectra of the samples were obtained with a UV-vis spectrometer (UV-2600, Shimadzu) equipped with a diffuse reflectance measurement unit (ISR-2600PLUS, Shimadzu) in which barium sulfate ($BaSO_4$) was used as a reference. Powder X-ray diffraction (XRD) with Cu-Kα radiation was recorded on MultiFlex diffractometer equipped with a carbon monochromator (Rigaku, Osaka). X-ray absorption spectroscopy (XAS) measurements were performed at BL-9C of the Photon Factory, Institute of Material Structure Science (KEK-IMSS-PF, Japan). Cr K-edge X-ray absorption near edge structure (XANES) spectra were recorded in fluorescence mode at room temperature using an Si(111) double crystal monochromator. Higher harmonics were removed by 50% detuning of the parallelism of the Si(111) crystals. Prior to measurements, XANES spectra of Cr_2O_3 and $Cr(OH)_3$, which were diluted by

boron nitride to give a proper absorption edge jump, and Cr foil were acquired in transmittance mode as a reference.

2.3. Water oxidation over TiO_2, $Cr(OH)_3/TiO_2$, Au/TiO_2 and $Cr(OH)_3/Au/TiO_2$ under irradiation of visible light

Dried photocatalyst powder (100 mg) and lanthanum oxide (FUJIFILM Wako Pure Chemical, Tokyo) (50 mg) was suspended in 10 mM silver nitrate ($AgNO_3$) aqueous solution (5 cm^3) in a test tube, bubbled with Ar, and sealed with a rubber septum. The suspension was irradiated with visible light of a xenon (Xe) lamp (Eagle Engineering, Tokyo) filtered with a Y48 filter (AGC Techno Glass) (450–800 nm: 580 mW cm^{-2}) with magnetic stirring in a water bath continuously kept at 293 K. The amount of O_2 in the gas phase was measured using a Shimadzu GC-8A gas chromatograph equipped with an MS-5A column. Silver metal deposited on the photocatalyst was dissolved with nitric acid, and the amount of Ag^+ was determined with atomic absorption spectrometry (AA-6200, Shimadzu).

2.4. Water splitting over Au/TiO_2 and $Cr(OH)_3/Au/TiO_2$ under irradiation of visible light

Powder of each of the samples (Au/TiO_2 and $Cr(OH)_3/Au/TiO_2$; 150 mg) was suspended in pure water (90 cm^3) by using a magnetic stirrer in a Pyrex side-irradiation vessel connected to a glass closed gas circulation system. The suspension was evacuated under vacuum several times to completely remove any residual air. A small amount of Ar gas was introduced into the reaction system prior to irradiation from a Xe lamp filtered with a Y48 filter. The amounts of H_2 and O_2 in the gas phase were measured using a Shimadzu GC-8A gas chromatograph equipped with an MS-5A column.

2.5. Photodeposition of lead oxide (PbO_2)

Fifty mg of $Cr(OH)_3/Au/TiO_2$ powder was suspended in 10 mM of lead(II) nitrate ($Pb(NO_3)_2$) aqueous solution (5 cm^3) in a test tube, bubbled with O_2, and sealed with a rubber septum. The suspension was irradiated with visible light of a Xe lamp filtered with a Y48 filter with magnetic stirring in a water bath continuously kept at 293 K. After 5 h of visible light irradiation, the suspension was filtered with a glass filter and washed with distilled water and then dried at 298 K in vacuo for 2 h. The resultant powder was observed with TEM.

2.6. Action spectrum

To obtain an action spectrum, some band pass filters (Asahi spectra, Tokyo, center wavelength: 452(HMZ0450), 499(HMZ0500), 551(HMZ0550), 602(HMZ0600), 651(HMZ0650), 698(HMZ0700) and 749(HMZ0750) nm) with light width of ±10 nm were attached to the Xe lamp. The intensity of light passing was determined by using a USR-45D spectroradiometer (Ushio, Tokyo). The number of photons was calculated from the intensity and the wavelength of light passing. Photocatalytic water oxidation reactions were conducted under the same conditions as those described above (experimental section 2.3.) except for the filters attached to the Xe lamp. Apparent quantum efficiency (AQE) at each centered wavelength of light was calculated from the ratio of four times the amount of O_2 and the amount of photons irradiated using the following Equation (1):

$$\mathrm{AQE} = \frac{4 \times \text{the amount of } O_2 \text{ evolved}}{\text{the amount of incident photons}} \times 100$$

Results and discussion

3.1. Photoabsorption (extinction) property

Figure 1 shows photoabsorption spectra of TiO_2, Au/TiO_2, $Cr(OH)_3/TiO_2$ and $Cr(OH)_3(y)/Au/TiO_2$ samples (y= 0.10, 0.20, 0.25, 0.50 and 1.00 wt%), in which the y-axis is shown with Kubelka-Munk (KM) function. Bare TiO_2 exhibited only absorption at λ< 400 nm due to the band gap excitation. In the spectrum of $Cr(OH)_3/TiO_2$, weak photoabsorption due to $Cr(OH)_3$ was observed at around 600 nm, which is attributed to the d–d transition of Cr^{3+}.[34] Strong photoabsorption was observed at around 550 nm in the spectra of Au/TiO_2 and $Cr(OH)_3(y)/Au/TiO_2$, which is attributed to LSPR of the supported Au NPs. The intensity of photoabsorption of LSPR was almost unchanged until y= 0.10 and then decreased when y> 0.10, though the amount of Au was constant (1.0 wt%). These results indicate that the effect of $Cr(OH)_3$ on LSPR was negligible until y=0.10 and that there is some interaction between Au NPs and $Cr(OH)_3$ at y> 0.10.

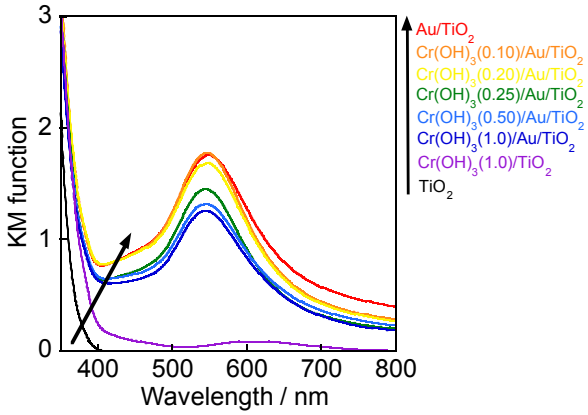

Figure 1. Photoabsorption spectra of TiO_2, Au/TiO_2, $Cr(OH)_3(y)/Au/TiO_2$, and $Cr(OH)_3/TiO_2$.

3.2. TEM observation

Figure 2 shows TEM images of Au/TiO_2 and $Cr(OH)_3(y)/Au/TiO_2$. Particle size distribution and average particle diameter determined from TEM observation are shown in Figure S1 (ESI†) and Table 1, respectively. Gold NPs were observed in the TEM image of Au/TiO_2 and the average size was determined to be 11.8 nm, indicating that Au NPs were successfully deposited on TiO_2 by the PD method. The average particle diameter of $Cr(OH)_3(y)/Au/TiO_2$ gradually increased with increase in the $Cr(OH)_3$ content until y= 0.25 and the value was almost constant (*ca*. 14.8 ± 0.1 nm) after y= 0.25. Since introduction of $Cr(OH)_3$ to Au/TiO_2 was performed at room temperature, there is no increase in particle size due to

sintering of Au NPs. Therefore, it can be concluded that the increase in the average size of NPs after introduction of $Cr(OH)_3$ was due to the deposition of $Cr(OH)_3$ on Au NPs. The thickness of the $Cr(OH)_3$ layer was calculated by Equation (2) and the values are shown in Table 1:

(Thickness of $Cr(OH)_3$ layer) = {(particle size of $Cr(OH)_3$/Au)-(particle size of Au)}/2 (2)

Since the $Cr(OH)_3$ shell was very thin and was not observed clearly in TEM photographs, an energy-dispersive X-ray spectrometer (EDS) was used to determine the deposition site of $Cr(OH)_3$. Figure S2 (ESI†) shows TEM images and EDS spectra of Au/TiO_2, $Cr(OH)_3(0.10)/Au/TiO_2$ and $Cr(OH)_3(1.0)/Au/TiO_2$. The results indicate that the particle in the center of the TEM photograph was Au and that $Cr(OH)_3$ was deposited on Au. In figure S2(c), a slight increase in the base line of the EDS spectra of Cr shows that a part of $Cr(OH)_3$ was also loaded on TiO_2 ,i.e., the amount of $Cr(OH)_3$ deposited on Au was limited.

Table 1. Effects of the amount of $Cr(OH)_3$ on the particle size of $Cr(OH)_3$/Au loaded on TiO_2 and thickness of the $Cr(OH)_3$ shell.

$Cr(OH)_3$ / wt%	Particle size / nm	Thickness of $Cr(OH)_3$ shell / nm
0	11.8	-
0.10	12.3	0.3
0.20	12.9	0.6
0.25	14.9	1.6
0.50	14.8	1.5
1.0	14.7	1.5

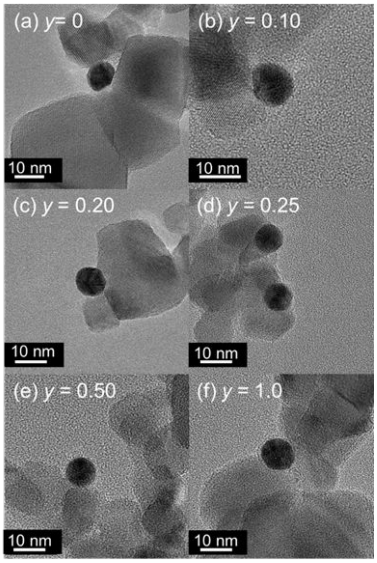

Figure 2. TEM images of (a) Au/TiO_2 and (b)-(f) $Cr(OH)_3(y)/Au/TiO_2$.

3.3. Electron state

X-ray photoelectron spectroscopy (XPS) was used to obtain information on changes in the electron states of Au NPs by modification with $Cr(OH)_3$. Figure 3 shows Au 4f XPS spectra of Au/TiO_2, $Cr(OH)_3(y)/Au/TiO_2$ and $Cr(OH)_3/TiO_2$. Two peaks due to Au $4f_{7/2}$[35] and Au $4f_{5/2}$[36] were observed in spectra of Au/TiO_2 and $Cr(OH)_3(y)/Au/TiO_2$, while no peaks were observed in the spectrum of $Cr(OH)_3/TiO_2$. Peaks assignable to Au^0 were observed at 84.0 and 87.4 eV in the spectrum of Au/TiO_2 and peaks for $Cr(OH)_3(0.050)/Au/TiO_2$ were observed at the same positions. We noted that the peaks shifted to 83.0 and 86.6 eV when 0.10 wt% $Cr(OH)_3$ was introduced to Au/TiO_2. As shown in Figure S3 (ESI†), we confirmed that the binding energy values of C 1s, Ti 2p, and O 1s did not change even in the increase in the amount of $Cr(OH)_3$. Therefore, the shift of the Au 4f peaks to a lower binding energy means that Au of $Cr(OH)_3(0.10)/Au/TiO_2$ was in an electron-rich state, *i.e.*, electrons were donated from the $Cr(OH)_3$ layer to Au. Further increase in the $Cr(OH)_3$ content (≥ 0.20 wt%) did not cause a further shift. An electron-rich state is preferable for a plasmonic photocatalytic reaction because injection of electrons from Au NPs to the conduction band of TiO_2 becomes easier.

Since peaks of the Cr 2p XPS spectrum appeared at a region similar to that in the Ti 2p XPS spectrum, the electron state of $Cr(OH)_3$ was unclear (Figure S4, ESI†). Therefore, we measured Cr K-edge XANES spectra to determine the chemical states of $Cr(OH)_3$. Figure 4 shows Cr K-edge XANES spectra of $Cr(OH)_3(0.10)/Au/TiO_2$ (red line), $Cr(OH)_3$ (blue line), Cr_2O_3 (green line), and Cr foil (black line). The spectra of $Cr(OH)_3$ and Cr_2O_3 were similar to those reported for $Cr(OH)_3$ and Cr_2O_3.[37] The Cr K-edge spectrum of $Cr(OH)_3(0.10)/Au/TiO_2$ was similar to that of $Cr(OH)_3$, indicating that the oxidation state and coordination state of Cr species of $Cr(OH)_3(y)/Au/TiO_2$ are close to those of $Cr(OH)_3$. Domen's group reported that a Cr species loaded on Rh NPs was identified as Cr_2O_3 having a corundum structure and that Cr_2O_3 at the outer surface was hydrated to a $CrO_{(1.5-m)}(OH)_{2m}{\cdot}xH_2O$ layer in an aqueous medium.[38, 39] Pang *et al.*[40] reported that the Cr species of an Ag core-Cr shell cocatalyst loaded on Ga_2O_3 had a $Cr(OH)_3$ structure based on XANES analysis. In the XRD pattern of $Cr(OH)_3(0.10)/Au/TiO_2$ (Figure S5, ESI†), only peaks due to the anatase and rutile phases were observed because of the small loading of $Cr(OH)_3$ and Au.

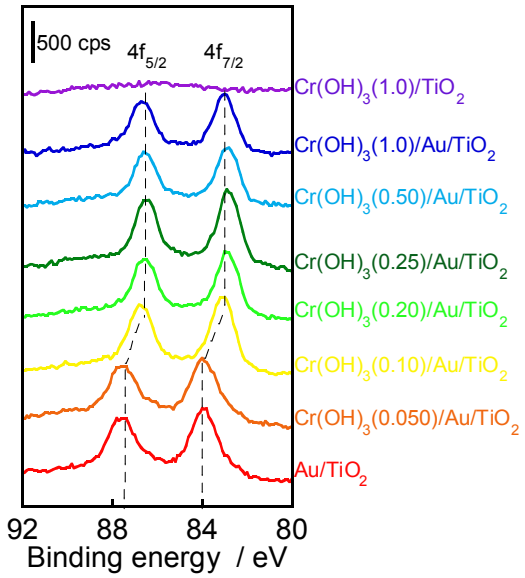

Figure 3. XPS spectra of Au/TiO_2, $Cr(OH)_3/TiO_2$ and $Cr(OH)_3(y)/Au/TiO_2$ around the Au 4f component.

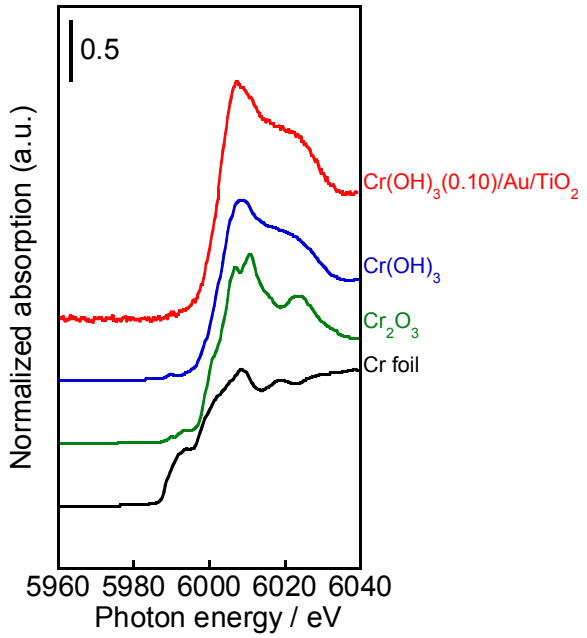

Figure 4. Cr K-edge XANES spectra of Cr foil (black line), Cr_2O_3 (green line), $Cr(OH)_3$ (blue line) and $Cr(OH)_3(0.10)/Au/TiO_2$ (red line).

3.4. Water oxidation reaction

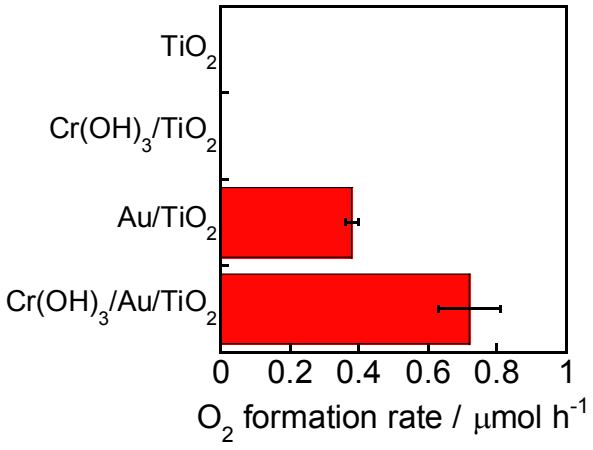

Figure 5. Rates of O_2 formation in aqueous suspensions of various photocatalysts under irradiation of visible light from a Xe lamp equipped with a Y48 cut-filter.

Four samples (TiO_2, $Cr(OH)_3(0.10)/TiO_2$, $Au(1.0)/TiO_2$ and $Cr(OH)_3(0.10)/Au(1.0)/TiO_2$) were used for O_2 production by water oxidation in the presence of Ag^+ as an electron scavenger under irradiation of visible light. Figure 5 shows the rates of O_2 evolution of these samples. No O_2 was produced over TiO_2 and $Cr(OH)_3/TiO_2$ because no band-gap excitation occurred under irradiation of visible light. On the other hand, water was oxidized over Au/TiO_2 under visible light irradiation, resulting in plasmonic O_2 evolution, as was reported previously in the presence of another electron scavenger.[25] We noted that introduction of $Cr(OH)_3$ increases the rate by two fold (0.38 μmol h^{-1} to 0.72 μmol h^{-1}), *i.e.*, $Cr(OH)_3$ strongly contributes to the water oxidation over Au/TiO_2. We further investigated the effect of $Cr(OH)_3$ on plasmonic O_2 evolution as described in the next section in order to clarify the function of $Cr(OH)_3$.

Figure 6 shows the time course of O_2 formation from an aqueous $AgNO_3$ solution in the presence of $Cr(OH)_3(0.10)/Au/TiO_2$ under the same conditions as those in the experiment for which results are shown in Figure 5. In the reaction system, Ag^+ was reduced by photogenerated electrons, resulting in deposition of Ag metal on the surface of the photocatalyst. Figure 6 also shows the amount of Ag deposited on $Cr(OH)_3(0.10)/Au/TiO_2$. The amounts of O_2 evolved and Ag deposited increased linearly with prolongation of photoirradiation time. After irradiation of visible light for 3 h, 2.3 μmol of O_2 and 9.4 μmol of Ag were produced. Redox balance (ROB) of this reaction was calculated from Equation (3):

$$ROB = n[Ag] / 4n[O_2], \quad (3)$$

where $n[Ag]$ and $n[O_2]$ are the amounts of Ag and O_2 formed during the photocatalytic reaction. The values of ROB during the reaction for 3 h were almost unity, indicating that reduction of Ag^+ and oxidation of water occurred stoichiometrically as shown in Equation (4):

$$2H_2O + 4Ag^+ \longrightarrow O_2 + 4Ag + 4H^+. \quad (4)$$

Analysis of the filtrate after the photocatalytic reaction for 3 h with an inductively coupled plasma optical emission spectrometer in JRC revealed that dissolution of Cr species was under the detection limit, indicating that the $Cr(OH)_3$ shell on Au is stable under the reaction condition of this study.

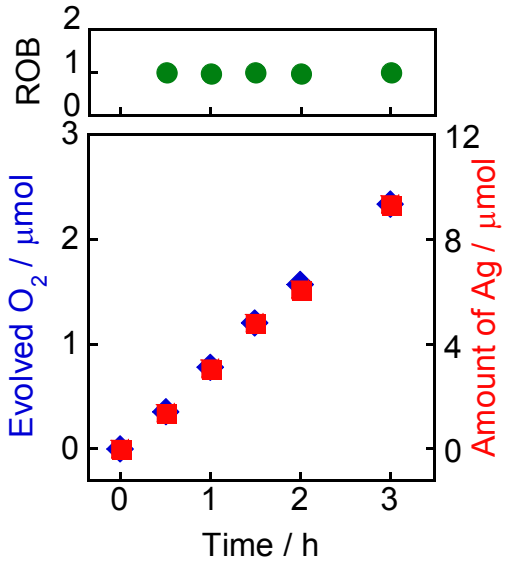

Figure 6. Time courses of the amounts of O_2 evolved and Ag deposited in an aqueous suspension of $Cr(OH)_3(0.10)/Au/TiO_2$ under irradiation of visible light from a Xe lamp equipped with a Y48 cut-filter.

Figure 7 shows the effect of the amount of $Cr(OH)_3$ (y) on the O_2 evolution rate over $Cr(OH)_3(y)/Au(1.0)/TiO_2$. The rate of O_2 formation over Au/TiO_2 (without $Cr(OH)_3$ modification) was 0.38 μmol h^{-1} as shown in Figure 5. Only a small amount of $Cr(OH)_3$ loading (y= 0.050 wt%) increased the formation rate and the rate increased to 0.72 μmol h^{-1} until y = 0.10 wt%. A further increase in y decreased the rate. There seems to be two reasons for the decrease of O_2 formation rate: (1) $Cr(OH)_3$

loaded on Au NPs negatively affected LSPR and (2) $Cr(OH)_3$ loaded on TiO_2 surface suppressed reduction of Ag^+ to Ag. Since the $Cr(OH)_3$ shell of $Cr(OH)_3(0.10)/Au(1.0)/TiO_2$ was very thin as shown in Figure 1 and Table 1, the negative effect of the $Cr(OH)_3$ shell on LSPR was negligible. Decrease in LSPR of $Cr(OH)_3/Au(1.0)/TiO_2$ having a larger $Cr(OH)_3$ content ($y > 0.10$ wt%) partly accounts for the results. In addition, $Cr(OH)_3$ was deposited on the TiO_2 surface as well as Au NPs as shown in Figure S2. To evaluate the role of $Cr(OH)_3$ loaded on TiO_2, O_2 production over TiO_2 and $Cr(OH)_3(1.0$ wt%$)/TiO_2$ in the presence of $AgNO_3$ under irradiation of UV light from a high pressure mercury lamp was examined (Figure S6). The O_2 formation rate over $Cr(OH)_3(1.0$ wt%$)/TiO_2$ (0.068 μmol min^{-1}) was smaller than that over TiO_2 (0.20 μmol min^{-1}), indicating that the thicker $Cr(OH)_3$ layer on the TiO_2 surface suppressed reduction of Ag^+ to Ag.

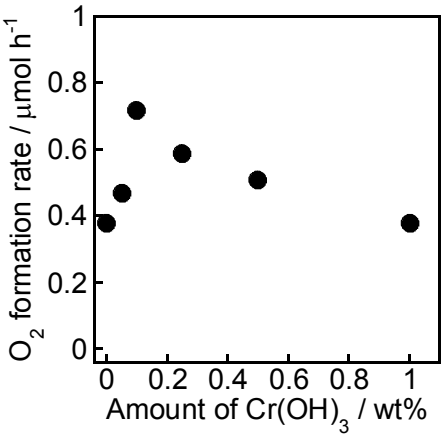

Figure 7. Effects of the amount of $Cr(OH)_3$ on O_2 formation rates over Au/TiO_2 and $Cr(OH)_3(y)/Au/TiO_2$ under irradiation of visible light from a Xe lamp equipped with a Y48 cut-filter.

3.5. Water splitting

We previously reported stoichiometric water splitting over Au/TiO_2 samples under irradiation of visible light.[24] It is known that H_2 evolution over bare TiO_2 is generally difficult and that a cocatalyst for H^+ reduction is indispensable, although the potential of the conduction band of TiO_2 (*ca.* -0.2 V_{NHE} at pH 0) is electrochemically sufficient for proton reduction (0 V_{NHE} at pH 0). Therefore, in the case of water splitting over an Au/TiO_2 plasmonic photocatalyst, Au NPs also work as a cocatalyst for reduction of H^+. However, the reaction rate of water splitting over Au/TiO_2 was small and introduction of an NiO_x cocatalyst was effective for water splitting.[24] Another strategy to improve the activity of water splitting is acceleration of water oxidation. The results presented in the previous section showed that modification of Au NPs with $Cr(OH)_3$ increased the rate of plasmonic water oxidation. Au/TiO_2 and $Cr(OH)_3(0.10)/Au/TiO_2$ were therefore used for water splitting under irradiation of visible light in the absence of an electron accepter. Figure 8(a) shows rates of formation of H_2 and O_2 over Au/TiO_2 with and without a $Cr(OH)_3$ shell. As also reported previously, Au/TiO_2 was active in water splitting and, as expected, $Cr(OH)_3(0.10)/Au/TiO_2$ showed reaction rates two-times larger than those of Au/TiO_2. Since $Cr(OH)_3$ did not work as a cocatalyst for H_2 production, the increase in the reaction rate of water splitting was caused by improvement of water oxidation by $Cr(OH)_3$. Figure 8(b) shows time courses of the amounts of H_2 and O_2 produced from an aqueous suspension of $Cr(OH)_3(0.10)/Au/TiO_2$ under visible light irradiation. The amounts of H_2 and O_2 increased linearly with prolongation of photoirradiation time. The ratio of yields of H_2 and O_2 (H_2/O_2) was calculated from Equation (5):

$$H_2/O_2 = n(H_2)/n(O_2), \quad (5)$$

where $n(H_2)$ and $n(O_2)$ are the amounts of H_2 and O_2 during the photocatalytic reaction, respectively. The value of H_2/O_2 was almost 2.0 regardless of irradiation time (Figure 8(b), right axis), indicating that H_2 and O_2 evolution from water occurred with a high stoichiometry, as shown in Equation (6):

$$2H_2O \longrightarrow 2H_2 + O_2. \quad (6)$$

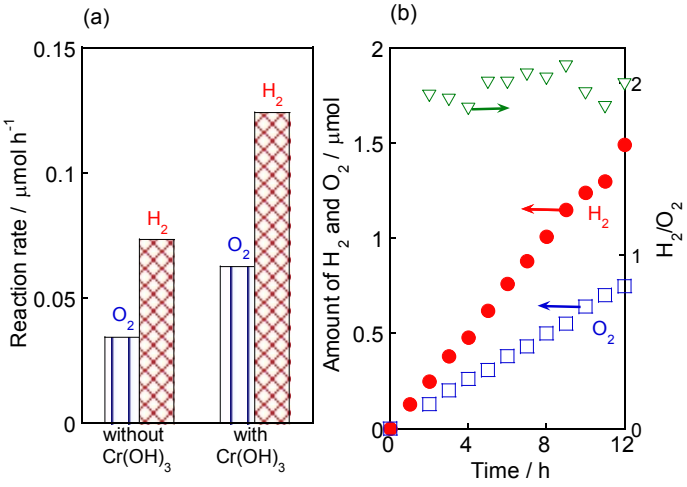

Figure 8. (a) H_2 and O_2 formation rates over Au/TiO_2 with and without a $Cr(OH)_3$ shell under irradiation of visible light, (b) Time courses of evolution of H_2 and O_2 from water and the ratio over $Cr(OH)_3(0.10)/Au/TiO_2$ under irradiation of visible light from a Xe lamp equipped with a Y48 cut-filter.

3.6. Action spectrum

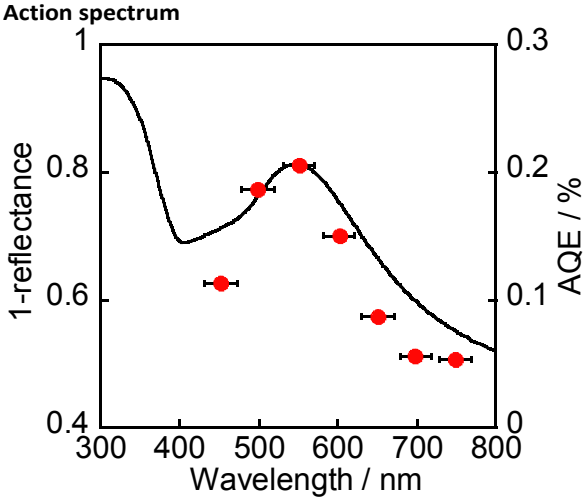

Figure 9. Action spectrum of $Cr(OH)_3(0.10)/Au/TiO_2$ in O_2 evolution from aqueous $AgNO_3$ (10 mM).

We measured an action spectrum to determine whether O_2 was produced via a band-gap-induced process, an LSPR-induced (plasmonic) process or a thermocatalytic process. Figure 9 shows the extinction spectrum of $Cr(OH)_3(0.10)/Au/TiO_2$ (left axis) and AQE (right axis). The action spectrum showed a

tendency similar to that of the extinction spectrum of $Cr(OH)_3(0.10)/Au/TiO_2$ and we therefore concluded that O_2 formation from water proceeds via a plasmonic process. The values of AQE at 550 nm and 750 nm were 0.21% and 0.054%, respectively. However, these values are still small and should be improved by a new method for introduction of $Cr(OH)_3$ to Au.

3.7. Investigation on reaction sites

To obtain information on the reduction and oxidation sites of $Cr(OH)_3(0.10)/Au/TiO_2$, two reactions in which one of the reduced and oxidized products was deposited on the photocatalyst were examined.[41] The first reaction was water oxidation in the presence of Ag^+, which was discussed in Figure 6 (Equation (4)), in which Ag metal was deposited. The half reaction is shown in Equation (7) and the position of Ag means the place where photogenerated electrons accumulate, *i.e.*, the reduction sites of $Cr(OH)_3(0.10)/Au/TiO_2$:

$Ag^+ + e^- \longrightarrow Ag$. (7)

Figure S7(a) (ESI†)shows a TEM image of $Cr(OH)_3(0.10)/Au/TiO_2$ after the water oxidation. Fine particles were observed on TiO_2 in addition to Au NPs (*ca.* 11 nm). TEM observation (Figure 2 and Figure S7(a)) indicated that the fine particles deposited on TiO_2 are Ag metal and that reduction of Ag^+ occurs on TiO_2.

The second reaction was oxidation of Pb^{2+} in the presence of O_2. The reaction is expressed by Equation (8):

$Pb^{2+} + H_2O + 1/2O_2 \longrightarrow PbO_2 + 2H^+$. (8)

The half reaction is shown in Equation (9) and the position of PbO_2 means the place where positive holes accumulate, *i.e.*, the oxidation sites of $Cr(OH)_3(0.10)/Au/TiO_2$:

$Pb^{2+} + 2H_2O + 2h^+ \longrightarrow PbO_2 + 4H^+$. (9)

In the TEM image of $Cr(OH)_3(0.10)/Au/TiO_2$ after the reaction (Figure S7(b), ESI†), a new shell was observed on $Cr(OH)_3$/Au particles. Since the $Cr(OH)_3$ layer on Au particles was too thin (0.3 nm) to be observed (Figure 2(b)), the new shell is assignable to the species produced by the photocatalytic reaction. Figure S8 (ESI†) shows the results of Pb 4f XPS of $Cr(OH)_3(0.10)/Au/TiO_2$ after the photocatalytic reaction. Peaks due to Pb ($4f_{5/2}$ and $4f_{7/2}$) were observed at 143.3 and 138.4 eV, which were assignable to Pb^{4+}.[42] These results support the idea that the species deposited on $Cr(OH)_3$/Au particles was PbO_2, *i.e.*, oxidation of Pb^{2+} took place on $Cr(OH)_3$. To determine the place where the oxidation of Pb^{2+} occurred, $Cr(OH)_3(0.10)/Au/TiO_2$ after the reaction was analyzed by using EDS. In the line maps of Au, Cr and Pb (Figure S9, ESI†), the peak due to Pb was observed at the same place at which the peaks due to Au and Cr were observed, indicating that the new shell was PbO_2 and that photocatalytic oxidation of Pb^{2+} to PbO_2 occurs on $Cr(OH)_3$/Au NPs.

3.8. Function of $Cr(OH)_3$ and working mechanism

From the positions of the reduced product (Ag) and oxidized product (PbO_2), we obtained information about the transfer of electrons and holes over $Cr(OH)_3/Au/TiO_2$ under irradiation of visible light. It is generally accepted that photogenerated electrons are injected into the conduction band of semiconductors having Au NPs. Furube *et al.*[43] reported that photogenerated electrons transfer from Au nanodots to TiO_2 within 240 fs. Therefore, the reduction site of $Cr(OH)_3(0.10)/Au/TiO_2$ is the surface of TiO_2. Formation of PbO_2 shows that the oxidation site of $Cr(OH)_3(0.10)/Au/TiO_2$ is the surface of $Cr(OH)_3$, which also indicates that positive holes transfer from Au NPs to $Cr(OH)_3$. Very recently, the effect of hole transfer in plasmon-induced charge separation was proposed.[44] Based on the results of this study, the proposed mechanisms of water oxidation and water splitting over $Cr(OH)_3/Au/TiO_2$ are shown in Figure 10. Water oxidation in the presence of Ag^+ consists of four steps (Figure 10a): (1) holes (h^+) and electrons (e^-) are generated through LSPR excitation,[45, 46,47, 48, 49] (2) photoexcited e^- are injected from Au NPs into the conduction band of TiO_2[43, 50] and used for reduction of Ag^+, resulting in the deposition of Ag on the surface of TiO_2, (3) photogenerated h^+ are transferred to the surface of the $Cr(OH)_3$ shell and accept electrons from water, resulting in O_2 evolution, and (4) Au NPs return to the original state through the hole transfer. Tatsuma *et al.*[32] employed $Ni(OH)_2$ and CrO_x as p-type materials for a TiO_2/Au electrode to fabricate n-M-p (ohmic) and n-M-p (Schottky) structures, respectively, and they concluded that $Ni(OH)_2$ is more suitable for charge accumulation. Sekizawa *et al.*[30] reported that a thin Cr_2O_3 layer inserted between an N, Zn-Fe_2O_3 photocathode and the conductive oxide layer ensured efficient electron transfer and generated a favorable band alignment for hole transfer. These reports support process (3). The increase in the rate of O_2 formation is explained by efficient charge separation due to transformation of photogenerated h^+ to the surface of $Cr(OH)_3$.

In the case of water splitting, *i.e.*, in the absence of Ag^+ in water, the processes except process (2) are the same in the presence of Ag^+ (Figure 10b). Generally, a cocatalyst is required for H_2 evolution by H^+ reduction with photoexcited e^- in the conduction band of TiO_2 because the position of the conduction band is close to the reduction potential of H^+. In our previous study on the effect of a cocatalyst on plasmonic H_2 production, we found that Au NPs loaded on TiO_2 also act as a cocatalyst.[25] Similarly, Au NPs also act as sites for H_2 formation in water splitting. It is known that the both the $CrO_{(1.5-m)}(OH)_{2m}\cdot xH_2O$ layer and the $Cr(OH)_3$ layer are permeable to H^+ and H_2.[34-38] We also evaluated the H_2 evolution over $Cr(OH)_3/Au/TiO_2$ and Au/TiO_2 through the band-gap excitation mechanism under UV light irradiation (Figure S10, ESI†). The rates of H_2 evolution became smaller by modifying $Cr(OH)_3$ because $Cr(OH)_3$ limited the access of H^+ to Au. The results support the conclusion that the improved photocatalytic activity for water splitting by modifying $Cr(OH)_3$ was derived from the efficient charge separation due to the transformation of h^+ to $Cr(OH)_3$.

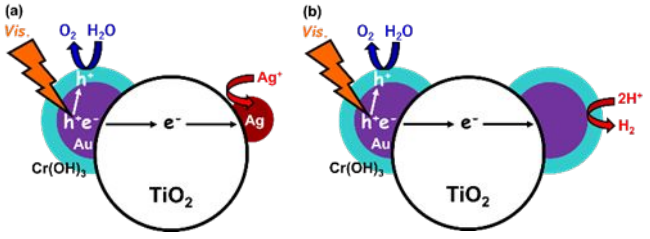

Figure 10. Schematic illustrations of mechanisms for (a) plasmonic water oxidation and (b) plasmonic water splitting over $Cr(OH)_3/Au/TiO_2$ under irradiation of visible light.

Conclusions

By using a PD method, a Cr species was successfully introduced to Au/TiO_2. TEM observation and EDS analysis revealed that a thin layer of the Cr species formed on Au NPs. When 0.10 wt% of the Cr species was introduced, the layer was very thin (*ca*. 0.3 nm) and the layer did not alter the photoabsorption (extinction) due to LSPR of Au NPs. Cr K-edge XANES spectra clarified that the oxidation state and coordination state of the Cr species loaded on Au/TiO_2 are close to those of $Cr(OH)_3$. XPS analysis showed that Au of $Cr(OH)_3/Au/TiO_2$ samples having y= 0.10 or more was in an electron-rich state, *i.e.*, electrons were donated from the $Cr(OH)_3$ layer to Au.

Formation of a very thin $Cr(OH)_3$ shell on Au NPs was effective for hole transfer in plasmonic photocatalytic reactions. In plasmonic water oxidation under irradiation of visible light in the presence of a sacrificial reagent, the rate of O_2 formation increased by two fold by modifying Au/TiO_2 with 0.10 wt% $Cr(OH)_3$. In plasmonic water splitting free from a sacrificial reagent, the reaction rate over $Cr(OH)_3(0.10)/Au/TiO_2$ was 1.6-times than that over Au/TiO_2.

Results of oxidative deposition of PbO_2 revealed that plasmonic oxidation occurs on $Cr(OH)_3/Au$ and that $Cr(OH)_3$ effectively works as a hole transfer cocatalyst. Based on the results, reaction mechanisms of plasmonic water oxidation and water splitting over $Cr(OH)_3/Au/TiO_2$ are proposed. In the case of water splitting, Au NPs also act as sites for H_2 formation.

Author Contributions

Eri Fudo: Investigation, Design of study, Acquisition of data, Analysis of data, Writing of original draft, Funding acquisition, Final approval of the article

Atsuhiro Tanaka: Conception of study, Funding acquisition, Analysis of data, Revising the manuscript, Final approval of the article

Shoji Iguchi: Acquisition of data, Analysis and interpretation of data, Final approval of the article

Hiroshi Kominami: Conception of study, Interpretation of data, Funding acquisition, Revising the manuscript critically for important intellectual content, Final approval of the article

Conflicts of interest

There are no conflicts to declare.

Acknowledgements

This work was partly supported by JSPS KAKENHI Grant Numbers 20H02527, 17H03462 and 17H04967 and the Precursory Research for Embryonic Science and Technology (PRESTO), supported by the Japan Science and Technology Agency (JST). E. F. is grateful to JSPS for a Research Fellowship for young scientists (No. 20J22342). A. T. is grateful for financial support from the Faculty of Science and Engineering, Kindai University and the Nippon Sheet Glass Foundation for Materials Science and Engineering. The XAFS study was performed under the approval of the Photon Factory Program Advisory Committee (Proposal No. 2019G629).

Notes and references

1. A. Kudo and Y. Miseki, *Chem Soc Rev*, 2009, **38**, 253-278.
2. K. Domen, A. Kudo and T. Onishi, *Journal of Catalysis*, 1986, **102**, 92-98.
3. H. Kato and A. Kudo, *chemical Physics Letters*, 1998, **295**, 487-492.
4. Y. Miseki, H. Kato and A. Kudo, *Chemistry Letters*, 2006, **35**, 1052-1053.
5. K. Meyer, M. Ranocchiari and J. A. van Bokhoven, *Energy & Environmental Science*, 2015, **8**, 1923-1937.
6. K. Sayama, K. Mukasa, R. Abe, Y. Abe and H. Arakawa, *Chem Commun (Camb)*, 2001, DOI: 10.1039/b107673f, 2416-2417.
7. K. Sayama, K. Mukasa, R. Abe, Y. Abe and H. Arakawa, *Journal of Photochemistry and Photobiology A: Chemistry*, 2002, **148**, 71-77.
8. M. Yagi, A. Syouji, S. Yamada, M. Komi, H. Yamazaki and S. Tajima, *Photochem. Photobiol. Sci.*, 2009, **8**, 139-147.
9. F. Jiao and H. Frei, *Energy & Environmental Science*, 2010, **3**, 1018-1027.
10. K. Maeda, K. Ishimaki, Y. Tokunaga, D. Lu and M. Eguchi, *Angew Chem Int Ed Engl*, 2016, **55**, 8309-8313.
11. E. Kowalska, O. O. Mahaney, R. Abe and B. Ohtani, *Phys Chem Chem Phys*, 2010, **12**, 2344-2355.
12. H. Kominami, A. Tanaka and K. Hashimoto, *Chem Commun (Camb)*, 2010, **46**, 1287-1289.
13. H. Kominami, A. Tanaka and K. Hashimoto, *Applied Catalysis A: General*, 2011, **397**, 121-126.
14. A. Tanaka, K. Hashimoto and H. Kominami, *ChemCatChem*, 2011, **3**, 1619-1623.
15. A. Tanaka, A. Ogino, M. Iwaki, K. Hashimoto, A. Ohnuma, F. Amano, B. Ohtani and H. Kominami, *Langmuir*, 2012, **28**, 13105-13111.
16. S. Naya, M. Teranishi, T. Isobe and H. Tada, *Chem Commun (Camb)*, 2010, **46**, 815-817.
17. A. Tanaka, K. Hashimoto and H. Kominami, *Chem Commun (Camb)*, 2011, **47**, 10446-10448.
18. A. Tanaka, K. Hashimoto and H. Kominami, *J Am Chem Soc*, 2012, **134**, 14526-14533.
19. C. u. G. Silva, R. J. rez, T. Marino, R. Molinari and H. Garcı´a, *Journal of the American Chemical Society*, 2011, **133**, 595-602.
20. H. Yuzawa, T. Yoshida and H. Yoshida, *Applied Catalysis B: Environmental*, 2012, **115-116**, 294-302.
21. A. Tanaka, S. Sakaguchi, K. Hashimoto and H. Kominami, *Catalysis Science & Technology*, 2012, **2**, 907-909.
22. A. Tanaka, S. Sakaguchi, K. Hashimoto and H. Kominami, *ACS Catalysis*, 2012, **3**, 79-85.
23. X. Ke, X. Zhang, J. Zhao, S. Sarina, J. Barry and H. Zhu, *Green Chem.*, 2013, **15**, 236-244.
24. A. Tanaka, K. Teramura, S. Hosokawa, H. Kominami and T. Tanaka, *Chem Sci*, 2017, **8**, 2574-2580.
25. A. Tanaka, K. Nakanishi, R. Hamada, K. Hashimoto and H. Kominami, *ACS Catalysis*, 2013, **3**, 1886-1891.

26. S. Wang, Y. Gao, S. Miao, T. Liu, L. Mu, R. Li, F. Fan and C. Li, *J Am Chem Soc*, 2017, **139**, 11771-11778.
27. H. Minamimoto, T. Toda, R. Futashima, X. Li, K. Suzuki, S. Yasuda and K. Murakoshi, *The Journal of Physical Chemistry C*, 2016, **120**, 16051-16058.
28. Y. Nishijima, K. Ueno, Y. Kotake, K. Murakoshi, H. Inoue and H. Misawa, *J Phys Chem Lett*, 2012, **3**, 1248-1252.
29. E. Nurlaela, H. Wang, T. Shinagawa, S. Flanagan, S. Ould-Chikh, M. Qureshi, Z. Mics, P. Sautet, T. Le Bahers, E. Cánovas, M. Bonn and K. Takanabe, *ACS Catalysis*, 2016, **6**, 4117-4126.
30. K. Sekizawa, K. Oh-ishi, K. Kataoka, T. Arai, T. M. Suzuki and T. Morikawa, *Journal of Materials Chemistry A*, 2017, **5**, 6483-6493.
31. J. Hu, C. Zha, H. Gao, L. Zeng, Y. Du and M. Zhu, *Sustainable Energy Fuels*, 2019, **3**, 439-449.
32. K. C. Kao, H. Nishi and T. Tatsuma, *ChemNanoMat*, 2019, **5**, 1021-1027.
33. M. Okazaki, Y. Suganami, N. Hirayama, H. Nakata, T. Oshikiri, T. Yokoi, H. Misawa and K. Maeda, *ACS Applied Energy Materials*, 2020, **3**, 5142-5146.
34. H. Wang, Y. Zhang, L. Zhang, Y. Guo, S. Liu, F. Gao, Y. Han, G. Feng, X. Liang and L. Ge, *RSC Advances*, 2016, **6**, 84871-84881.
35. W. McLean, C. A. Colmenares, R. L. Smith and G. A. Somorjai, *the Journal of Physical Chemistry*, 1983, **87**, 788-793.
36. N. H. Turner and A. M. Single, *Surface and Interface Analysis*, 1990, **15**, 215-222.
37. I. Tsuyumoto and Y. Maruyama, *Anal Chem*, 2011, **83**, 7566-7569.
38. K. Maeda, K. Teramura, D. Lu, N. Saito, Y. Inoue and K. Domen, *The Journal of Physical Chemistry C*, 2007, **111**, 7554-7560.
39. M. Yoshida, K. Takanabe, K. Maeda, A. Ishikawa, J. Kubota, Y. Sakata, Y. Ikezawa and K. Domen, *the Journal of Physical Chemistry C*, 2009, **113**, 10151-10157.
40. R. Pang, K. Teramura, H. Asakura, S. Hosokawa and T. Tanaka, *ACS Sustainable Chemistry & Engineering*, 2018, **7**, 2083-2090.
41. T. Ohno, K. Sarukawa and M. Matsumura, *New Journal of Chemistry*, 2002, **26**, 1167-1170.
42. B. Chen, W. Yan, Y. He, H. Huang, H. Leng, Z. Guo and J. Liu, *journal of the Electrochemical Society*, 2019, **166**, E119-E128.
43. A. Furube, L. Du, K. Hara, R. Katoh and M. Tachiya, *J Am Chem Soc*, 2007, **129**, 14852-14853.
44. T. Tatsuma and H. Nishi, *Nanoscale Horizon*, 2020, **5**, 597-606.
45. M. Xiao, R. Jiang, F. Wang, C. Fang, J. Wang and J. C. Yu, *Journal of Materials Chemistry A*, 2013, **1**, 5790-5805.
46. S. C. Warren and E. Thimsen, *Energy Environ. Sci.*, 2012, **5**, 5133-5146.
47. X. Zhou, G. Liu, J. Yu and W. Fan, *Journal of Materials Chemistry*, 2012, **22**, 21337–21354.
48. S. Linic, P. Christopher and D. B. Ingram, *Nat Mater*, 2011, **10**, 911-921.
49. T. Tatsuma, *Bulletin of the Chemical Society of Japan*, 2013, **86**, 1-9.
50. Y. Tian and T. Tatsuma, *J Am Chem Soc*, 2006, **127**, 7632-7637.